AMERICAN SOCIETY FOR MICROBIOLOGY | Journal of Virology®

STRUCTURE AND ASSEMBLY

Herpes Simplex Virus 1 UL34 Mutants That Affect Membrane Budding Regulation and Nuclear Lamina Disruption

Amber Vu,[a] Shaowen White,[b] Tiffany Cassmann,[b] Richard J. Roller[b]

[a]Department of Pediatrics, Carver College of Medicine, University of Iowa, Iowa City, Iowa, USA
[b]Department of Microbiology and Immunology, Carver College of Medicine, University of Iowa, Iowa City, Iowa, USA

ABSTRACT Nuclear envelope budding in herpesvirus nuclear egress may be negatively regulated, since the pUL31/pUL34 nuclear egress complex heterodimer can induce membrane budding without capsids when expressed ectopically or on artificial membranes *in vitro*, but not in the infected cell. We have previously described a pUL34 mutant that contained alanine substitutions at R158 and R161 and that showed impaired growth, impaired pUL31/pUL34 interaction, and unregulated budding. Here, we determine the phenotypic contributions of the individual substitutions to these phenotypes. Neither substitution alone was able to reproduce the impaired growth or nuclear egress complex (NEC) interaction phenotypes. Either substitution, however, could fully reproduce the unregulated budding phenotype, suggesting that misregulated budding may not substantially impair virus replication. In addition, the R158A substitution caused relocalization of the NEC to intranuclear punctate structures and recruited lamin A/C to these structures, suggesting that this residue might be important for recruitment of kinases for dispersal of nuclear lamins.

IMPORTANCE Herpesvirus nuclear egress is a complex, regulated process coordinated by two virus proteins that are conserved among the herpesviruses that form a heterodimeric nuclear egress complex (NEC). The NEC drives budding of capsids at the inner nuclear membrane and recruits other viral and host cell proteins for disruption of the nuclear lamina, membrane scission, and fusion. The structural basis of individual activities of the NEC, apart from membrane budding, are not clear, nor is the basis of the regulation of membrane budding. Here, we explore the properties of NEC mutants that have an unregulated budding phenotype, determine the significance of that regulation for virus replication, and also characterize a structural requirement for nuclear lamina disruption.

KEYWORDS herpes simplex, membrane budding, nuclear egress, nuclear lamina, protein kinases

During herpes simplex virus 1 (HSV-1) replication, newly constructed nucleocapsids escape from the nucleus to the cytoplasm via a process termed nuclear egress. Capsids dock at the inner nuclear membrane (INM), undergo envelopment and scission of the INM to create perinuclear enveloped virions (PEVs), and undergo deenvelopment at the outer nuclear membrane (ONM), allowing for capsid release into the cytoplasm (reviewed in reference 1). Viral proteins pUL31 and pUL34 form a heterodimeric core nuclear egress complex (NEC), and multimerization of this complex to form interacting hexameric rings is thought to drive membrane budding of the INM during nuclear egress (2–4). Accessory proteins, including the viral proteins pUS3, pUL47, ICP22, and ICP34.5 and the cellular proteins emerin, protein kinase Cδ (PKCδ), and p32, have been shown to interact with pUL31/pUL34 complexes, and some or all may form an extended NEC (5–13). These proteins play various roles in nuclear egress, including

Citation Vu A, White S, Cassmann T, Roller RJ. 2021. Herpes simplex virus 1 UL34 mutants that affect membrane budding regulation and nuclear lamina disruption. J Virol 95:e00873-21. https://doi.org/10.1128/JVI.00873-21.

Editor Richard M. Longnecker, Northwestern University

Address correspondence to Richard J. Roller, richard-roller@uiowa.edu.

Received 25 May 2021
Accepted 9 June 2021
Accepted manuscript posted online 16 June 2021
Published 10 August 2021

localized disruption of the nuclear lamina, regulation of deenvelopment, and other currently undefined events.

The nuclear lamina consists of networks of intermediate filament type lamin proteins that are anchored to the INM by interactions with INM-embedded lamin-associated proteins (LAPs) such as lamin B receptor (LBR), emerin, and others (reviewed in references 14 and 15). Disruption of the nuclear lamina is thought to assist herpesvirus nuclear egress in two ways. First, the meshwork of the lamina may present a steric barrier to capsid access to the INM (16). Second, connections between the lamins and LAPs may prevent the deformation of the INM that occurs during budding (17). HSVs disrupt the nuclear lamina, as shown by deformation of nuclear shape, redistribution of lamin proteins, and increased mobility of emerin and LBR (5–7, 13, 18–22). This is thought to occur by NEC-dependent recruitment of viral and cellular protein kinases, including pUS3 and PKCα, -β, and -δ, that phosphorylate both lamins and LAPs (6, 7, 13, 20). Recruitment of PKCδ has been shown to depend on the viral protein, ICP34.5 (13), and, in fact, it has not been shown that the NEC is sufficient to recruit any of the kinases that mediate lamina disruption.

Several lines of evidence suggest that the core NEC proteins, pUL31 and pUL34, are sufficient to drive membrane budding. The expression of pseudorabiesvirus (PRV) pUL31 and pU34 results in the pooling of vesicles in the perinuclear space (23). In addition, bacterially purified pUL31 and pUL34 cause vesicle formation when embedding into either giant unilamellar vesicles or liposomes (3, 4). During HSV-1 infection, however, membrane budding into the perinuclear space observed by transmission electron microscopy (TEM) occurs only in the context of capsid envelopment and creation of a PEV. This suggests that pUL31/pUL34-mediated membrane budding is negatively regulated and triggered by the capsid during infection.

We have previously characterized a charged cluster mutation of UL34, UL34(CL13), that performs uncoupled perinuclear budding of the INM (24). UL34(CL13) contains two mutations: one at amino acid 158 that changes arginine to alanine, generating pUL34$_{R158A}$, and one at amino acid 161 that changes arginine to alanine, generating pUL34$_{R161A}$. The CL13 double mutation caused a 100-fold reduction in virus production and a severe cell-cell spread defect. TEM of UL34-null virus-infected pUL34(CL13)-expressing cells displayed large invaginations of the INM that contained many dissimilar-sized vesicles that occasionally contained capsids in the perinuclear space.

We hypothesized that one or both of the CL13 substitutions uncouples budding from capsid envelopment and that this defect is responsible for the growth defect observed in infections with this mutant. We tested the effects of each of the pUL34$_{R158A}$ and pUL34$_{R161A}$ single mutations on the growth, spread, and promiscuous budding properties of UL34(CL13). Surprisingly, neither single mutation results in a cell-cell spread or growth defect, and yet both maintain the promiscuous budding phenotype of UL34 (CL13). In addition, we observed for the first time that ectopic expression of the NEC is sufficient to promote displacement of lamin proteins and that one of the CL13 mutations ablates that activity.

RESULTS

Mapping CL13 mutations onto the pUL31/pUL34 crystallized structure. Previous characterization of the UL34(CL13) mutant was performed before the crystal structure of the pUL31/pUL34 complex was solved. To determine whether the growth, spread, and promiscuous budding phenotypes of UL34(CL13) could be caused by destabilization of the pUL31/pUL34 complex, the R158A and R161A UL34 mutations were mapped onto the crystal structure (Fig. 1A). Mutation of amino acid 158 (arginine) to alanine is predicted to disrupt a salt bridge formation between UL34 residue R158 and UL31 residue D232 (Fig. 1B). The arginine residue 161 has no predicted interaction with pUL31 (Fig. 1C). These results suggest that the pUL34$_{R158A}$ substitution may play a role in disrupting pUL34 interaction with pUL31 but that the pUL34$_{R161A}$ substitution should have little effect on pUL34/pUL31 interaction. From this structural data, we

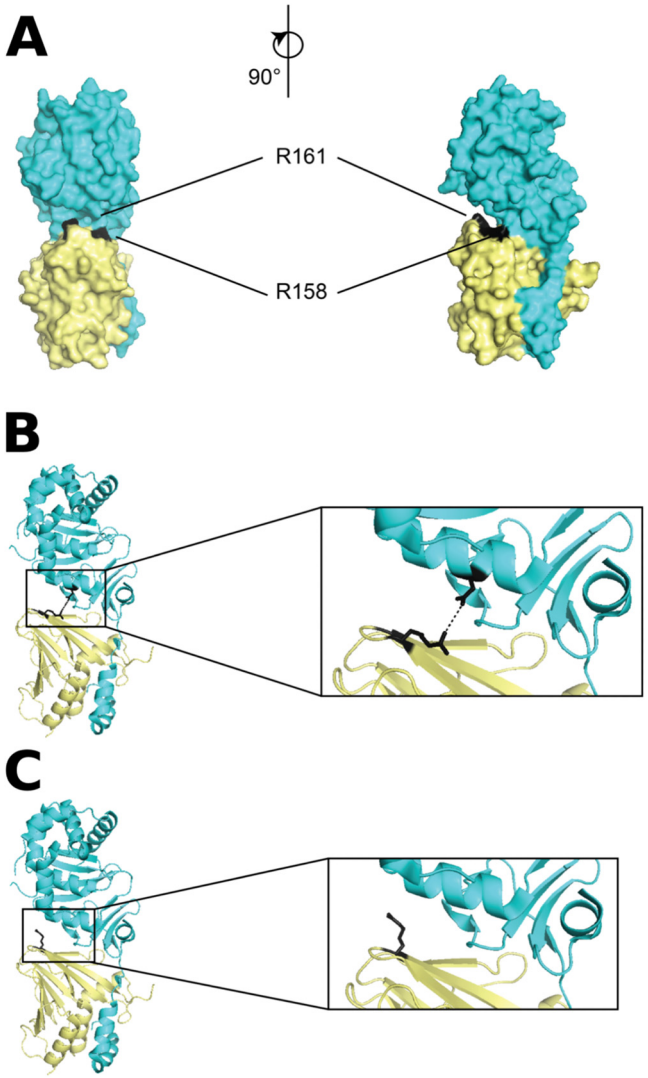

FIG 1 Position of R158 and R161 mutations. Atomic coordinate information from entry 4ZXS in the Research Collaboratory for Structural Bioinformatics Protein Data Bank (RCSB PDB) was rendered using MacPyMol. Only one of the two heterodimers is shown without accompanying ions or water molecules. (A) Space-filling rendering in two orientations of the crystal structure of the NEC heterodimer with pUL31 in teal and pUL34 in yellow. The positions of pUL34 residues R158 and R161 are indicated in black. (B) Ribbon rendering of the NEC heterodimer with expansion of the region around R158 showing positions of the side chain and putative salt bridge with pUL31 D232. (C) Same as panel B but illustrating the position of the side chain of R161.

hypothesized that pUL34$_{R158A}$ may be responsible for the growth, spread, and promiscuous budding phenotypes of UL34(CL13) as a result of destabilization of diminished pUL31/pUL34 interaction.

Effects of pUL34$_{R158A}$ and pUL34$_{R161A}$ single mutations on pUL31/pUL34 interaction. To determine the effect of the pUL34$_{R158A}$ and pUL34$_{R161A}$ single amino acid substitutions on pUL34 localization, an immunofluorescence-based colocalization assay was performed. Vero cells were transfected with pcDNA3 overexpression constructs carrying UL31-FLAG and constructs expressing hemagglutinin (HA)-tagged pUL34 wild-type (WT), pUL34(CL13), pUL34$_{R158A}$, or pUL34$_{R161A}$, and immunofluorescence was performed to determine colocalization of the two proteins (Fig. 2). Cells transfected with the plasmid containing pUL31-FLAG alone displayed typical pUL31 localization to the nucleoplasm (Fig. 2A). Cells transfected any of the HA-pUL34 plasmids alone displayed typical pUL34 localization to cytoplasmic membranes (Fig. 2B to E). pUL31-FLAG colocalized at the nuclear membrane when transfected with

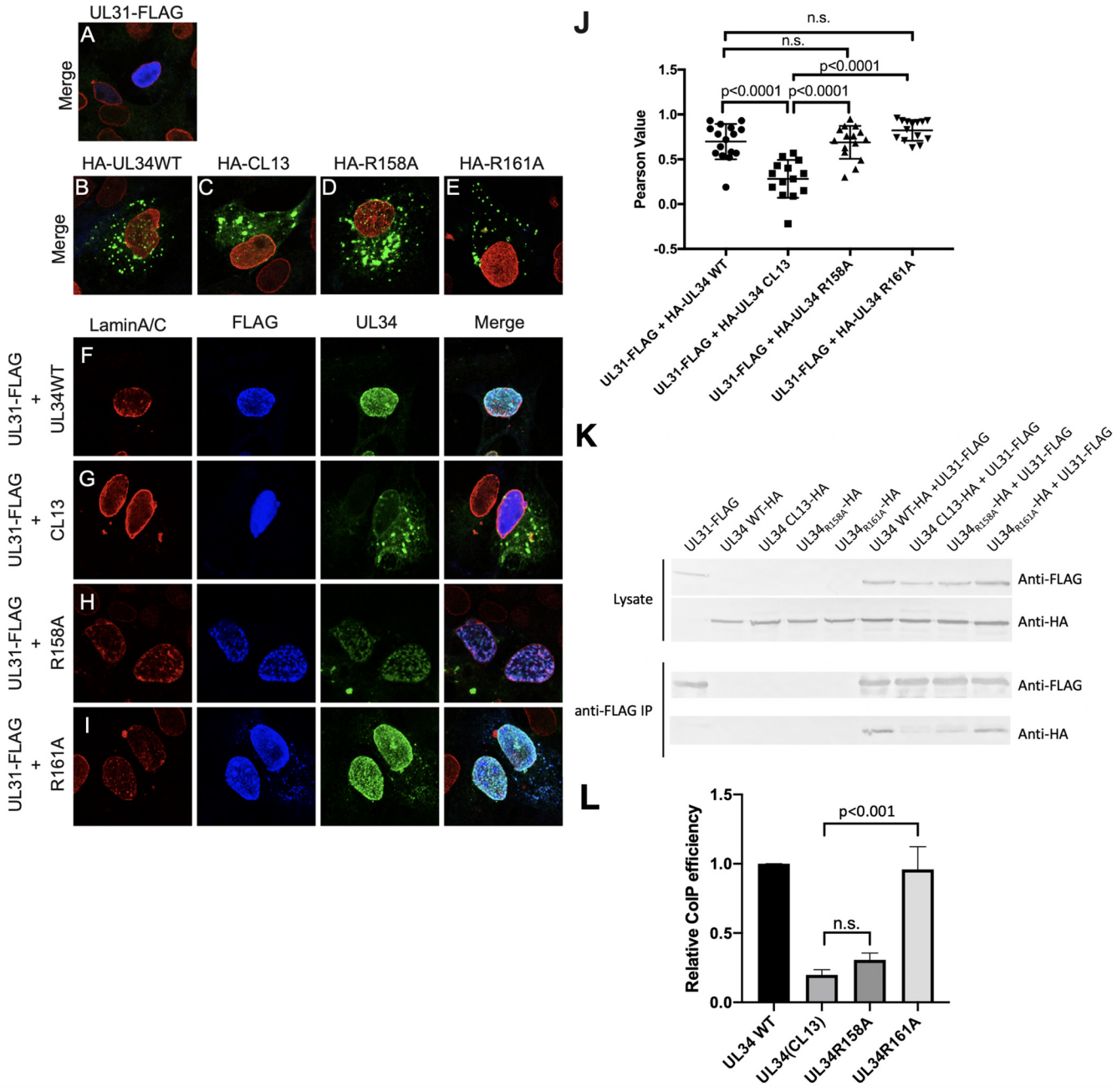

FIG 2 Interaction of UL34 mutants with pUL31. (A to E) Representative merged confocal images of Vero cells transfected with a construct carrying pUL31, pUL34WT, pUL34(CL13), pUL34$_{R158A}$, or pUL34$_{R161A}$ are shown. Cells were stained using antibodies against lamin A/C (red), FLAG (blue), and UL34 (green). (F to I) Representative confocal images showing Vero cells transfected with a construct carrying pUL31 and a construct encoding pUL31, pUL34WT, pUL34 (CL13), pUL34$_{R158A}$, or pUL34$_{R161A}$. Cells were fixed at 48 h posttransfection and stained for lamin A/C (first column, red), FLAG (second column, blue), and pUL34 (third column, green). (J) Colocalization of pUL31 and pUL34 was determined by calculating the Pearson's correlation coefficient. The statistical significance was determined by one-way analysis of variance (ANOVA) using the Tukey method for multiple comparisons implemented with GraphPad Prism. (K) Coimmunoprecipitation of pUL31-FLAG and pHA-UL34WT, pHA-UL34(CL13), pHA-UL34$_{R158A}$, and pHA-UL34$_{R161A}$. pUL31-FLAG was purified from 293T cells transfected with the indicated plasmid combinations. Immunoblots of cell lysates (top) and magnetic-bead purified samples (bottom) were incubated with antibodies against the HA or FLAG epitope. (L) Blot quantitation by densitometry of blots as shown in panel K expressed as the band intensity for each of the UL34 mutants divided by the band intensity for UL34 WT. The results are given as the mean and range of values for three independent experiments. Statistical significance was determined by one-way ANOVA using the Tukey method for multiple comparisons implemented with GraphPad Prism.

plasmids expressing HA-pUL34 WT or HA-pUL34$_{R161A}$ (Fig. 2F and I), indicating that the R161A mutation alone does not affect pUL31/pUL34 colocalization. As previously shown, little to no colocalization was observed in cells expressing both pUL31-FLAG and HA-pUL34(CL13), since pUL31-FLAG remained in the nucleoplasm and HA-pUL34(CL13) remained distributed

on cytoplasmic membranes with a small percentage at the nuclear membrane (Fig. 2G) (24). This lack of recruitment of both proteins to the nuclear periphery suggests that pUL31-FLAG and HA-pUL34(CL13) interact poorly with one another in the absence of other viral factors. Cells expressing both pUL31-FLAG and HA-pUL34$_{R158A}$ showed nontypical colocalization of the two proteins within large punctate structures in the nucleus and at the nuclear membrane (Fig. 2H). Colocalization of pUL31-FLAG with pUL34WT or the UL34 mutants was quantified by Pearson's correlation coefficient (Fig. 2J). Cells expressing pUL31-FLAG and HA-tagged pUL34 WT, pUL34$_{R158A}$, or pUL34$_{R161A}$ all have similar Pearson values above 0.5, indicating that these proteins colocalize (Fig. 2J). Cells expressing pUL31-FLAG and HA-pUL34(CL13) have significantly lower Pearson values below 0.5, demonstrating loss of colocalization. These data indicate that the inability of pUL34(CL13) to colocalize with pUL31 is not solely due the either the R158A or the R161A substitution alone.

To further determine the effect of the single UL34 mutations on pUL31/pUL34 interaction, coimmunoprecipitation was performed. 293T cells were transfected with the pUL31-FLAG construct and constructs expressing HA-tagged pUL34WT, pUL34(CL13), pUL34$_{R158A}$, or pUL34$_{R161A}$, and pUL31-FLAG were immunoprecipitated with anti-FLAG magnetic beads using limiting amounts of beads so that equivalent amounts of pUL31 were immunoprecipitated regardless of the amount present in the input. Consistent with strong colocalization during transfection, HA-tagged pUL34WT and pUL34$_{R161A}$ could both be efficiently coimmunoprecipitated with pUL31-FLAG. Surprisingly, despite relatively strong colocalization observed in Vero cells, the HA-tagged pUL34$_{R158A}$ mutant protein was coimmunoprecipitated inefficiently with pUL31, consistent with a significantly weaker interaction and suggesting that the R158A mutation may be largely responsible for the poor interaction between pUL31 and pUL34(CL13).

Effect of UL34$_{R158A}$ and UL34$_{R161A}$ single mutations on pUL34 recruitment to the nuclear membrane during infection. In transfected, uninfected cells, pUL34(CL13) is not recruited to the nuclear membrane to colocalize with pUL31 (Fig. 2). However, it has been previously shown that pUL34(CL13) regains the ability to be recruited to the nuclear membrane during infection (24). To further characterize the UL34$_{R158A}$ and UL34$_{R161A}$ single mutations, Vero cell lines that stably express these mutant proteins under an infection-inducible promoter were created. Expression of pUL34 was compared to HSV-1(F)-infected Vero cells by immunoblotting UL34-null virus-infected cellular lysates of cells that express pUL34WT, pUL34(CL13), pUL34$_{R158A}$, and pUL34R$_{161A}$, using ICP27 expression as a loading and infection control (Fig. 3A). The expression of all three of the mutant pUL34 proteins was comparable to that seen in HSV-1(F) infection. The pUL34WT cells expressed less pUL34 than the other cell types; however, this cell line has been previously characterized to complement UL34-null virus growth, cell-cell spread, and pUL31/pUL34 colocalization to nearly WT levels (25).

To determine the distribution of pUL34$_{R158A}$ and pUL34$_{R161A}$ during infection, Vero, WT, and mutant pUL34-expressing cells were infected with UL34-null virus and assayed by immunofluorescence for lamin A/C and pUL34 (Fig. 3B to H). At 15 h after infection pUL34 recruitment to the nuclear membrane was observed during a WT HSV-1(F) infection of Vero cells (Fig. 3C) and in pUL34WT-expressing cells infected with the UL34-null virus (Fig. 3E). In addition, pUL34$_{R158A}$ and pUL34$_{R161A}$ both localized to the nuclear periphery in a manner similar to wild-type during infection (Fig. 3G and H). As previously reported, CL13 pUL34 is also recruited to the nuclear rim, but to a lesser degree than the WT (Fig. 3F), and the completeness of recruitment was related to expression level of pUL34(CL13), with higher levels of expression associated with larger amounts of the mutant pUL34 on cytoplasmic membranes. The recruitment of CL13 pUL34 to the nuclear envelope in infected, but not transfected, cells suggests that viral factors in addition to pUL31 promote pUL34 recruitment to the nuclear periphery.

The localization of the three mutant pUL34 proteins to the nuclear membrane during infection suggested that interaction with pUL31 might also be promoted in infected cells. To test this, Vero, and WT and mutant pUL34-expressing cells were infected with a previously described UL31$_{R229L}$-FLAG/UL34-null virus (25). pUL31$_{R229L}$

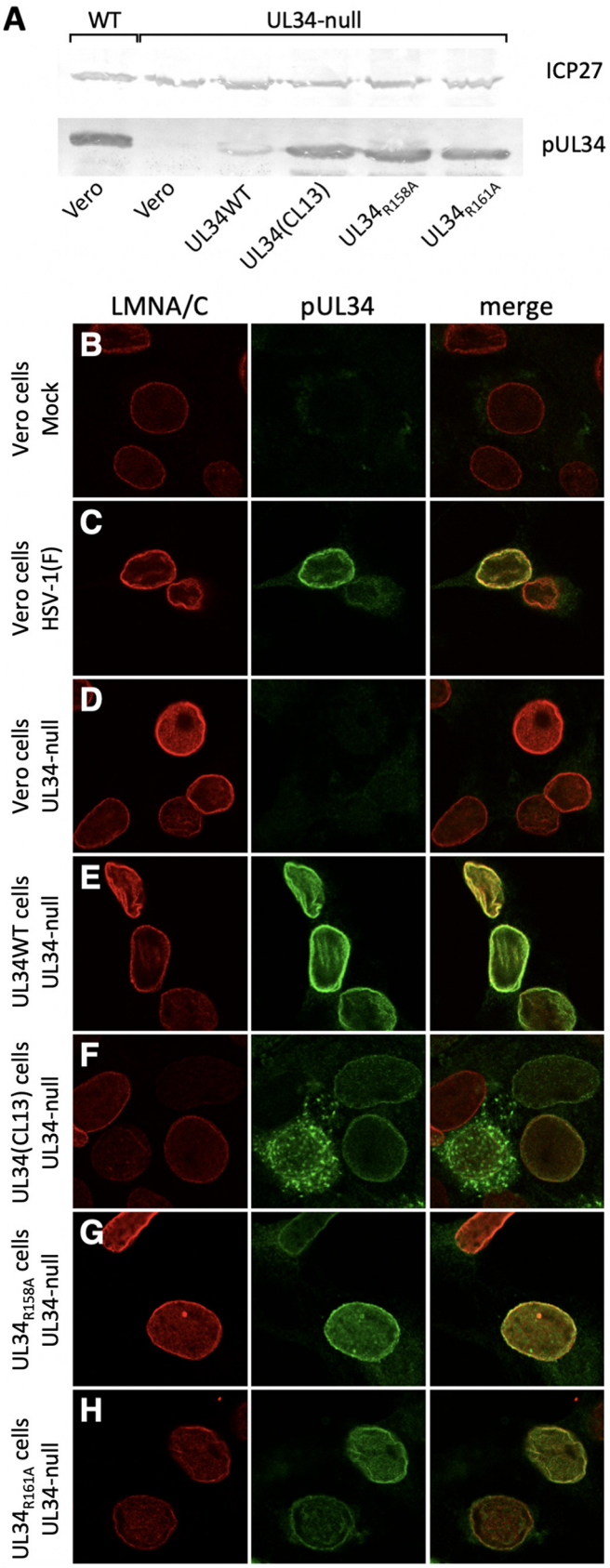

FIG 3 Localization of mutant pUL34 proteins in infected cells. (A) Digital image of immunoblots of lysates from cells that express no pUL34, pUL34 WT, or pUL34 mutants infected with wild-type or

(Continued on next page)

has been shown to interact pUL34 in a WT-like manner and is recruited normally to the nuclear periphery by pUL34 WT (25). Infection of this virus onto pUL34WT-expressing cells indeed displayed typical pUL31 recruitment to the nuclear periphery and colocalization with pUL34 (Fig. 4D). Interestingly, the localization of pUL31 in cells that express mutant pUL34 proteins still closely resembled that seen in transfected cells (Fig. 2). Very little pUL31 recruitment to the nuclear envelope was seen during infection of pUL34(CL13)-expressing cells (Fig. 4E), and pUL31 displayed a punctate nucleoplasmic pattern during infection of $pUL34_{R158A}$-expressing and $pUL34_{R161A}$-expressing cells (Fig. 4F and G). These data suggest that all three mutants alter interaction with pUL31 even in infected cells but that both the R158A and R161A mutations are required for the full impairment seen with the CL13 mutation.

Effects of $UL34_{R158A}$ and $UL34_{R161A}$ single mutations on virus growth and spread. To determine the role of $UL34_{R158A}$ and $UL34_{R161A}$ on virus production, 18-h transient and stable complementation growth assays were performed (Fig. 5). Vero cells were transfected with the UL34WT, UL34(CL13), $UL34_{R158A}$, or $UL34_{R161A}$ constructs and then infected with UL34-null virus 24 h after transfection. As previously described, the UL34 (CL13)-transfected sample supports growth very poorly and to the same extent as the untransfected control (24, 26) (Fig. 5A), whereas both single mutants showed intermediate complementation ability. Since neither of the single mutations complements as poorly as the UL34(CL13) double mutant, these data suggest that neither single mutation is solely responsible for the growth defect of UL34(CL13).

Single-step growth assays using the wild-type and mutant pUL34-expressing cell lines yielded slightly different results (Fig. 5B and C). All HSV-1(F)-infected cell lines produced similar viral titers, demonstrating that none of the mutant pUL34 proteins had a dominant negative effect on WT viral growth (Fig. 5B). Infection of the pUL34(CL13) cell line with UL34-null virus resulted in a significant ($P < 0.05$) ~20-fold decrease in virus titer compared to cells that expressed pUL34 WT at 18 and 24 h postinfection (hpi) that was nonetheless significantly greater ($P < 0.05$) than that from Vero cells that expressed no pUL34 (Fig. 5C). Single-step growth of UL34-null virus in the cell lines that expressed either of the two single mutants was not significantly different from growth in cells that expressed pUL34 WT at any time point (Fig. 5C). Interestingly, growth of UL34-null virus on cells that express pUL34R161A was significantly greater than on cells that express pUL34(CL13) and was reproducibly (but not significantly) greater than on cells that express WT pUL34, suggesting that the R161A mutation does not contribute to the growth phenotype of the double mutant. Growth of UL34-null virus on pUL34R158A-expressing cells was not significantly different from growth on cells that express either pUL34WT or pUL34(CL13), leaving open the possibility that this single mutation may have some effect on virus replication on its own. Altogether, these data suggest that neither of the $pUL34_{R158A}$ and $pUL34_{R161A}$ single substitutions can fully account for the growth defect caused by the double mutation.

pUL34 has been shown to have a cell-to-cell spread function in addition to its function in virus production (27, 28). The ability of the single and double mutant pUL34 proteins to support spread was determined using a plaque size assay on the mutant UL34-expressing cell lines (Fig. 6). The double mutant CL13 cell line supported spread no better than cells that expressed no pUL34 (Fig. 6F, H, and K). The single $pUL34_{R158A}$ and $pUL34_{R161A}$ mutant-expressing cell lines supported spread at least as well as the WT UL34-expressing cell line (Fig. 6G, I, J, and K). Overall, these data indicate that the 2-log reduction in plaque size caused by UL34(CL13) double mutation is not solely due to either of the $pUL34_{R158A}$ or the $pUL34_{R161A}$ single mutations.

FIG 3 Legend (Continued)
UL34-null virus and probed for ICP7 or pUL34. The virus used for infection is indicated above the blot images, and the cell line infected is indicated below. (B to H) Digital confocal images of cells lines that express no pUL34, pUL34 WT, or pUL34 mutants that were mock infected or infected with wild-type or UL34-null virus 16 h and then fixed and stained with antibodies directed against lamin A/C (red) or pUL34 (green). The identity of the cell line and virus used for infection is indicated to the left of each panel.

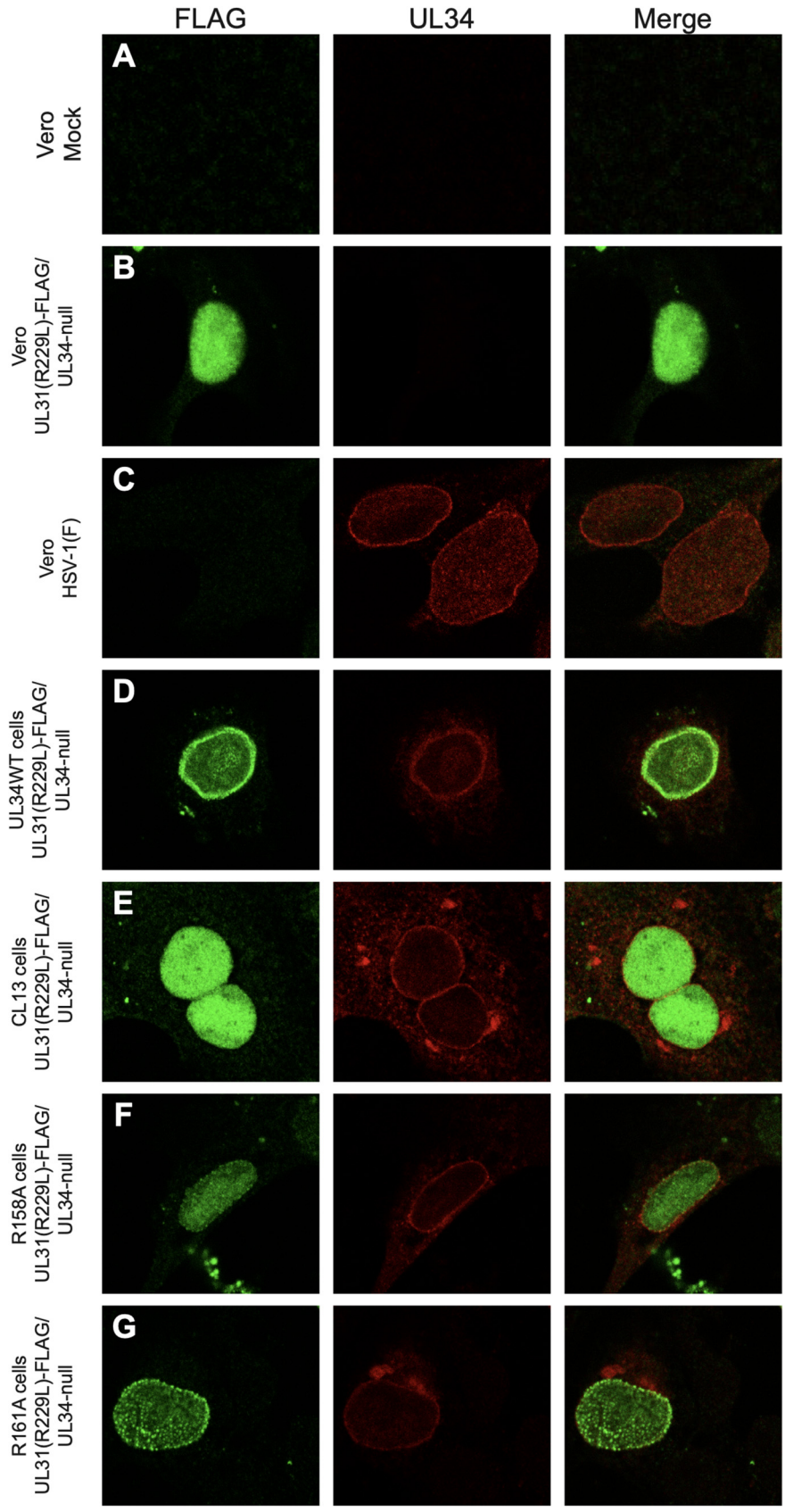

FIG 4 Localization of pUL31-FLAG and mutant pUL34 proteins in infected cells. Digital confocal images of cells lines infected with WT, UL34-null, or UL34-null/UL31$_{R229L}$-FLAG virus for 16 h and then fixed and

(Continued on next page)

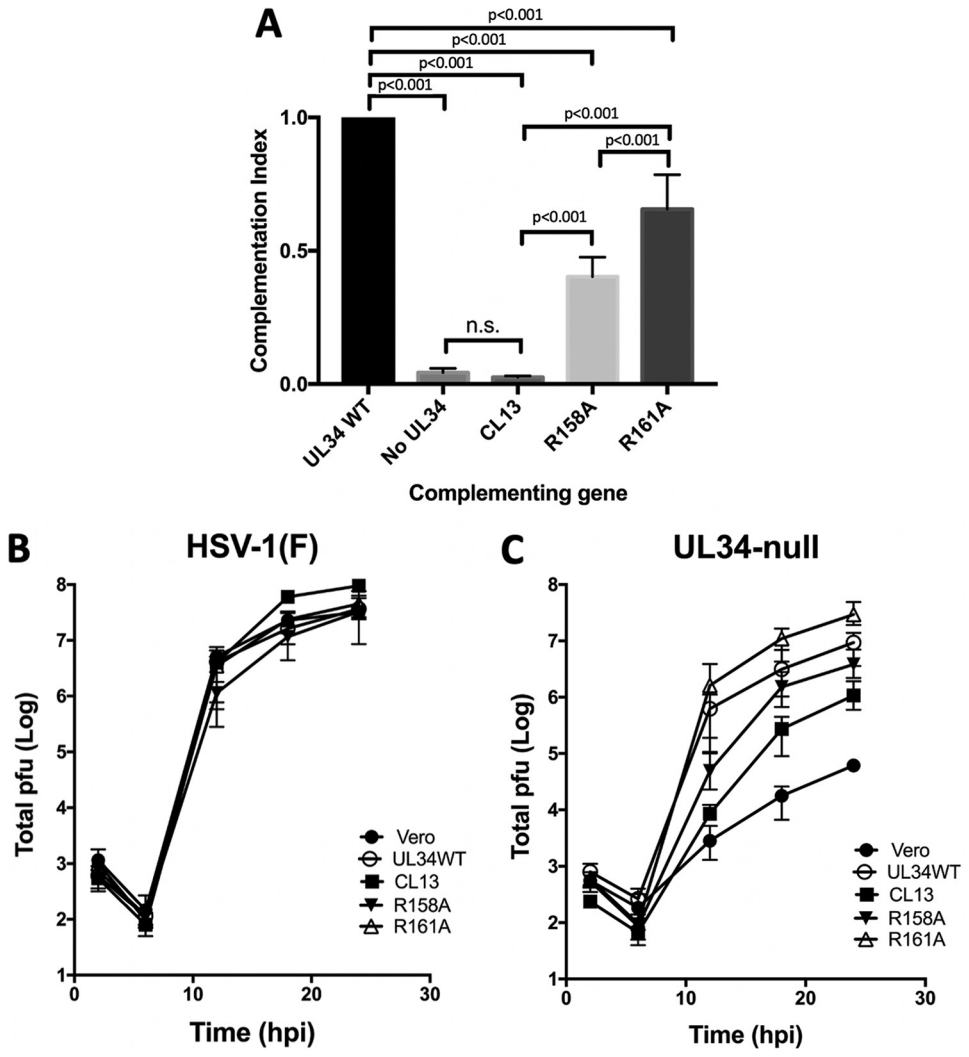

FIG 5 Effects of pUL34$_{R158A}$ and pUL34$_{R161A}$ on viral growth. (A) Transcomplementation of single-step UL34-null replication. Vero cells were transfected with pUL34WT-, pUL34(CL13)-, pUL34$_{R158A}$-, and pUL34$_{R161A}$-expressing plasmids under the control of the UL34 promoter/regulatory sequences. Transfected cells were subsequently infected with UL34-null virus, and at 18 hpi the amount of infectious virus produced was determined by plaque assay on UL34WT-complementing cells. Virus production was normalized for transfection efficiency, and the complementation index was calculated as the ratio of virus produced by the UL34WT-transfected cells. Statistical significance was determined by performing a one-way ANOVA using the Tukey method for multiple comparisons implemented on GraphPad Prism. (B and C) Single-step growth of WT and UL34-null virus on Vero, pUL34WT-expressing, pUL34(CL13)-expressing, pUL34$_{R158A}$-expressing, and pUL34$_{R161A}$-expressing cells. Each data point represents the mean of three independent experiments. Error bars in all panels represent the range of values obtained in three independent experiments. Statistical significance was determined by performing a one-way ANOVA on log-converted values from each time point using the Tukey method for multiple comparisons implemented on GraphPad Prism. Because of the density of the curves, significance is not indicated on the graph but is indicated in Results where appropriate.

Effect of pUL34$_{R158A}$ and pUL34$_{R161A}$ single substitutions on nuclear egress. Due to the ability of pUL34$_{R158A}$ and pUL34$_{R161A}$ to efficiently perform cell-cell spread and virus production, we hypothesized that neither of these mutations would cause the nuclear egress defect observed with the pUL34(CL13) double mutant (24). TEM analysis of Vero, pUL34WT-expressing, pUL34(CL13)-expressing, pUL34$_{R158A}$-expressing, and pUL34$_{R161A}$-expressing cells infected for 20 h with UL34-null virus revealed a significant nuclear egress

FIG 4 Legend (Continued)
stained with antibodies directed against FLAG epitope (green) or pUL34 (red). The identity of the cell line and virus used is indicated to the left of each panel. The images chosen are representative of at least 20 cells observed in at least three independent experiments.

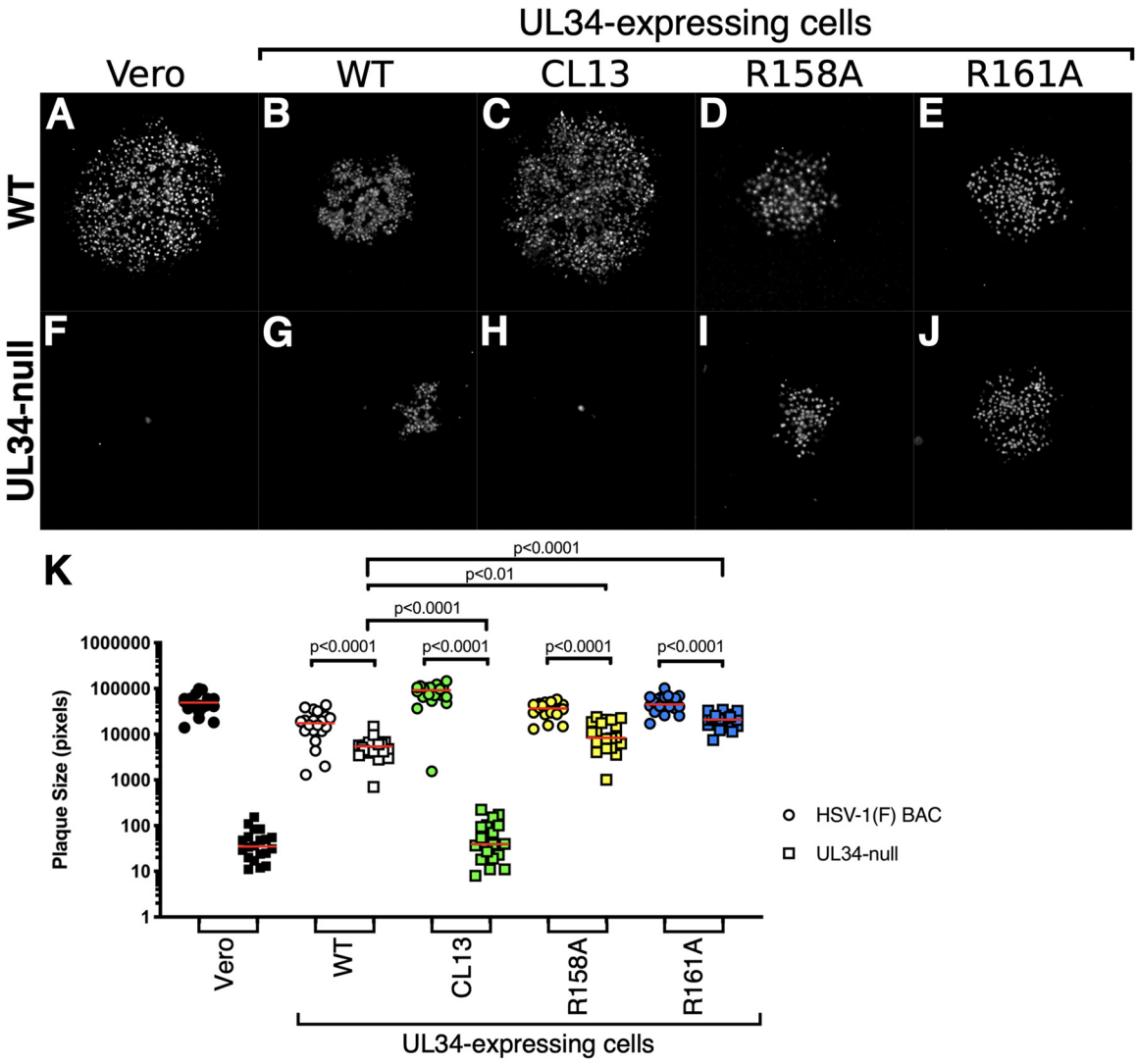

FIG 6 Effects of pUL34$_{R158A}$ and pUL34$_{R161A}$ on cell-to-cell spread. Plaque size assay of HSV-1(F) or UL34-null viruses on Vero, pUL34WT-expressing, pUL34(CL13)-expressing, pUL34$_{R158A}$-expressing, and pUL34$_{R161A}$-expressing cells. (A to J) representative images of plaques that were immunostained at 48 h after infection using antibody directed against the capsid scaffold protein. The cell line infected is indicated above the panels; the infecting virus is indicated to the left. (K) Plaque areas were measured 48 h after infection at a low MOI. Each point represents a single plaque area. A total of 20 plaques were measured for each condition. Statistical significance was determined by performing a Kolmogorov-Smirnov test in pairwise comparisons.

defect in CL13-expressing cells but not in cells that express either of the single mutants (Fig. 7). There were significantly more capsids in the nucleus and significantly fewer capsids in the extranuclear compartment of Vero and pUL34(CL13)-expressing cells compared to pUL34WT-expressing cells, suggesting a sequestration of capsids in the nucleus (Fig. 7A and C). In the extranuclear compartment, there was no significant difference in the percentage of capsids in UL34WT-expressing, pUL34$_{R158A}$-expressing, and pUL34$_{R161A}$-expressing cells, indicating that the single point mutants do not cause a nuclear egress defect (Fig. 7C). pUL34$_{R161A}$-expressing cells displayed significantly more capsids in the perinuclear space compared to the other cell types (Fig. 7B), suggesting the possibility that this mutation causes some impairment in deenvelopment.

To confirm the nuclear egress phenotype of pUL34$_{R158A}$ and pUL34$_{R161A}$, an RFP-VP26-tagged virus was used to measure the amount of capsid in the nuclear and cytoplasmic compartments by fluorescence analysis. Vero, pUL34WT-expressing, pUL34(CL13)-expressing, pUL34$_{R158A}$-expressing, and pUL34$_{R161A}$-expressing cells were infected with a UL34-null/RFP-VP26 virus or HSV-1(F)/RFP-VP26 virus and fixed 12 hpi. Cells were stained for host DNA

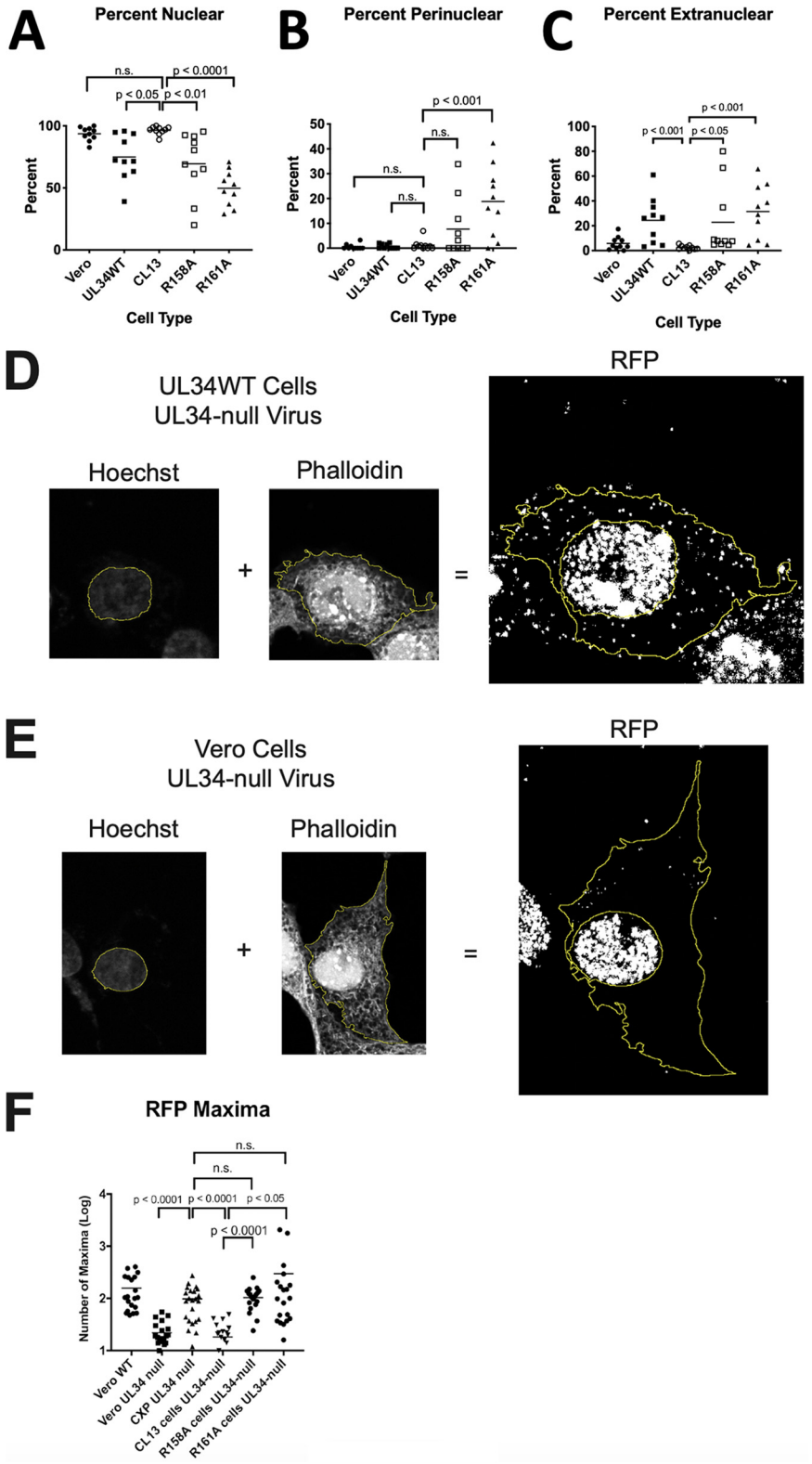

FIG 7 Effects of pUL34$_{R158A}$ and pUL34$_{R161A}$ on nuclear egress. (A to D) Total capsid quantification of TEM imaging. Capsids were counted in the nuclear (A), perinuclear (B), and extranuclear (C) compartments of pUL34WT-expressing, pUL34(CL13)-expressing, pUL34$_{R158A}$-expressing, and pUL34$_{R161A}$-expressing cells. Each point represents the number of capsids in the corresponding cellular compartment in a single cell. Statistical significance was calculated for pairwise comparisons by performing a Student *t* test. (D and E) Representative images of pUL34 WT-expressing (D) or Vero (E) cells showing staining with Hoechst and

(Continued on next page)

with Hoechst to indicate the nuclear boundary and with phalloidin to indicate the cytoplasm. RFP puncta presenting maximum intensity (termed RFP maxima) were quantified in the nuclear and total cellular (nucleus + cytoplasm) compartments and used to compute the number of cytoplasmic maxima (Fig. 7D and E). This method of RFP maxima quantitation ultimately underestimates the number of capsids in the cytoplasmic fraction due to some RFP puncta being below the threshold intensity, but the range of this assay is still large enough to distinguish gross differences in nuclear egress ability. As expected, UL34-null virus-infected Vero and pUL34(CL13)-expressing cells had many fewer cytoplasmic RFP maxima than the complementing UL34-null virus-infected pUL34WT-expressing cells (Fig. 7D to F). Consistent with the TEM capsid quantitation, UL34-null virus-infected pUL34$_{R158A}$-expressing and pUL34$_{R161A}$-expressing cells had comparable amounts of RFP maxima as UL34-null virus-infected pUL34WT-expressing cells (Fig. 7F). As a whole, the TEM capsid quantitation and RFP maxima assays show that the single mutants UL34$_{R158A}$ and UL34$_{R161A}$ are individually insufficient to cause the nuclear egress defect of UL34(CL13).

Effect of UL34$_{R158A}$ and UL34$_{R161A}$ single mutations on perinuclear vesicle formation during infection. To determine whether the UL34$_{R158A}$ or UL34$_{R161A}$ single mutation affects the coupling of perinuclear budding with capsid docking, TEM of Vero, pUL34WT-expressing, pUL34(CL13)-expressing, pUL34$_{R158A}$-expressing, and pUL34$_{R161A}$-expressing cells infected with UL34-null virus was performed, and cells were screened for the presence of perinuclear capsidless vesicles. The only perinuclear vesicles observed in pUL34WT-expressing cells contained capsids, were singular, and were rarely observed (Fig. 8A), whereas many perinuclear vesicles that did not contain capsids and were too small to contain capsids were observed in pUL34(CL13)-expressing cells (Fig. 8B and E). Surprisingly, both pUL34$_{R158A}$-expressing and pUL34$_{R161A}$-expressing cells contained the perinuclear vesicular inclusions observed in pUL34(CL13)-expressing cells (Fig. 8C and F and Fig. 8D, G, and H, respectively). These vesicles inside the inclusions were sometimes associated with capsids and were observed within the nucleus (Fig. 8F) or contiguous with the perinuclear space (Fig. 8G and H). These data show that either the UL34$_{R158A}$ mutation or the UL34$_{R161A}$ mutation is sufficient to cause promiscuous, uncoupled perinuclear budding and suggests that promiscuous budding does not contribute to the defects in nuclear egress or virus production seen with the CL13 double mutant.

Effects of UL34$_{R158A}$ and UL34$_{R161A}$ single mutations on lamin disruption function in Vero cells. Defects in nuclear egress can result from interruption in any of several steps in the process, including disruption of the nuclear lamina, capsid docking, membrane budding, and deenvelopment. The CL13 mutant is evidently not defective in budding ability, suggesting that it is defective in nuclear lamina disruption, capsid docking, or both. Disruption of the lamina results in a change in nuclear contour from ovoid to irregular, and this change is dependent on pUL34 expression and can be prevented by mutations in pUL34 (5, 17). Measurement of changes in nuclear contour in cells that express our mutant pUL34 proteins and were infected with UL34-null virus showed that changes in nuclear contour were diminished by the CL13 double mutant and, to a lesser degree, by the two single mutants (Fig. 9). The ability of pUL34(CL13) to promote alterations to nuclear shape during infection is defective, with nuclear contour ratios much higher than those seen with pUL34 WT (panel B), and no different from those seen in uninfected Vero cells (compare Fig. 9A, C, and F). In contrast, both UL34$_{R158A}$ and UL34$_{R161A}$ single point mutations show an intermediate phenotype, with contour ratios between those seen for wild-type and CL13 pUL34 (Fig. 9D, E, and F).

Differences in disruption of the nuclear lamina by pUL31 pUL34 complexes could also be observed in cells cotransfected with UL31 and UL34 (Fig. 10). Compared to untransfected cells (Fig. 10A), coexpression of wild-type pUL31 and pUL34 results in

FIG 7 Legend (Continued)
phalloidin used to define the cytoplasmic space in images and the localization of RFP-tagged capsids in the cytoplasm. (F) RFP maxima in the cytoplasm of cells that express no pUL34, pUL34 WT, and pUL34 mutants were counted and plotted to measure nuclear egress of capsids. Each point represents one cell. Statistical significance was calculated for pairwise comparisons using a Student *t* test.

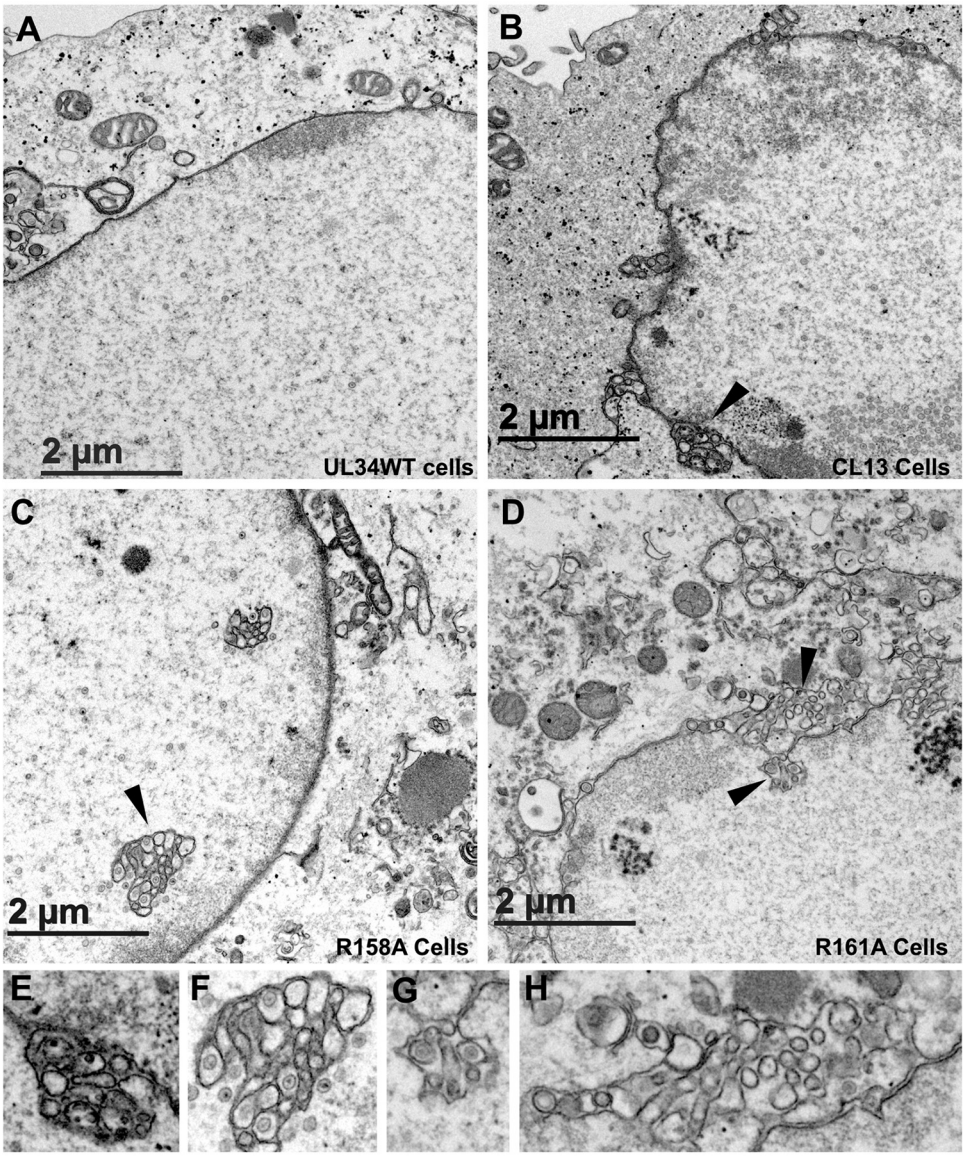

FIG 8 pUL34$_{R158A}$ and pUL34$_{R161A}$ mutants induce promiscuous budding. Digital images of cells that express pUL34WT (A), pUL34(CL13) (B and E), pUL34$_{R158A}$ (C and F) or pUL34$_{R161A}$ (D, G, and H) that were infected with pUL34-null virus for 20 h are shown. Concentrations of vesicles in the nucleus and the perinuclear space in panels A to D are indicated by arrowheads. (E to H) Enlargements of the regions indicated by the arrowheads in panels A to D.

the formation holes in the lamin A/C layer that coincide with the positions of NEC puncta in the nuclear envelope (Fig. 10B), suggesting that formation of NEC puncta causes displacement of lamin A/C in the absence of other viral factors. The same effect is observed in cells that coexpress pUL34$_{R161A}$, suggesting that this mutant NEC retains lamina dispersal activity (Fig. 10D). As shown above (Fig. 2), cotransfection of pUL31 and pUL34$_{R158A}$ results in formation of intranuclear NEC puncta (Fig. 10C). Surprisingly, however, lamin A/C concentrates at these same foci in cotransfected cells (Fig. 10C), resulting in significant colocalization of pUL34 and lamin A/C that is not seen with pUL34 wild type or pUL34$_{R161A}$ (Fig. 10D and E). A similar effect was seen on organization of lamin B, where expression of WT NEC results in formation of holes that coincide with NEC puncta (Fig. 10E). Expression of the R158A NEC also resulted in statistically significant colocalization with lamin B, but to a much lesser extent than seen for lamin A/C, requiring a more sensitive test for colocalization. These

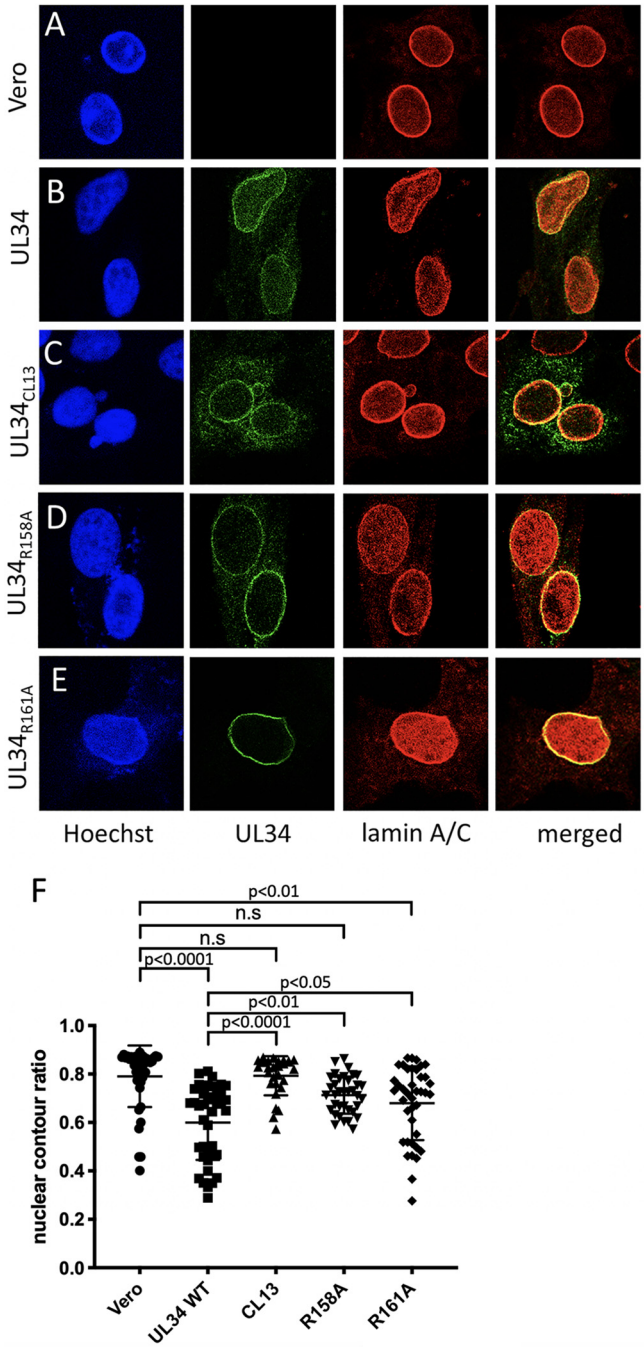

FIG 9 Effects of $pUL34_{R158A}$ and $pUL34_{R161A}$ on disruption of nuclear architecture. (A to E) Representative confocal images of cells that express no pUL34, pUL34 WT or pUL34 mutant infected for 16 h with UL34-null virus and then fixed and stained for DNA using Hoechst (blue) pUL34 (green) or lamin A/C (red). The cell line infected is indicated to the left of the panel. (F) Nuclear contour assay measuring the deviation of nuclear shape from circularity (lower values indicate a more convoluted nuclear shape). Each point represents a single nucleus, and 50 nuclei were measured. Statistical significance was determined by one-way ANOVA using the Tukey method for multiple comparisons implemented with GraphPad Prism. *P* values without brackets are relative to Vero cells.

results suggested the hypothesis that $pUL34_{R158A}$ is deficient in a lamin dispersal activity and that, in the absence of such activity, lamins may specifically and stably associate with the NEC.

Dispersal of lamins is associated with their phosphorylation, and the failure of the $UL34_{R158A}$ NEC to disperse lamins suggested that it might fail to recruit some host cell

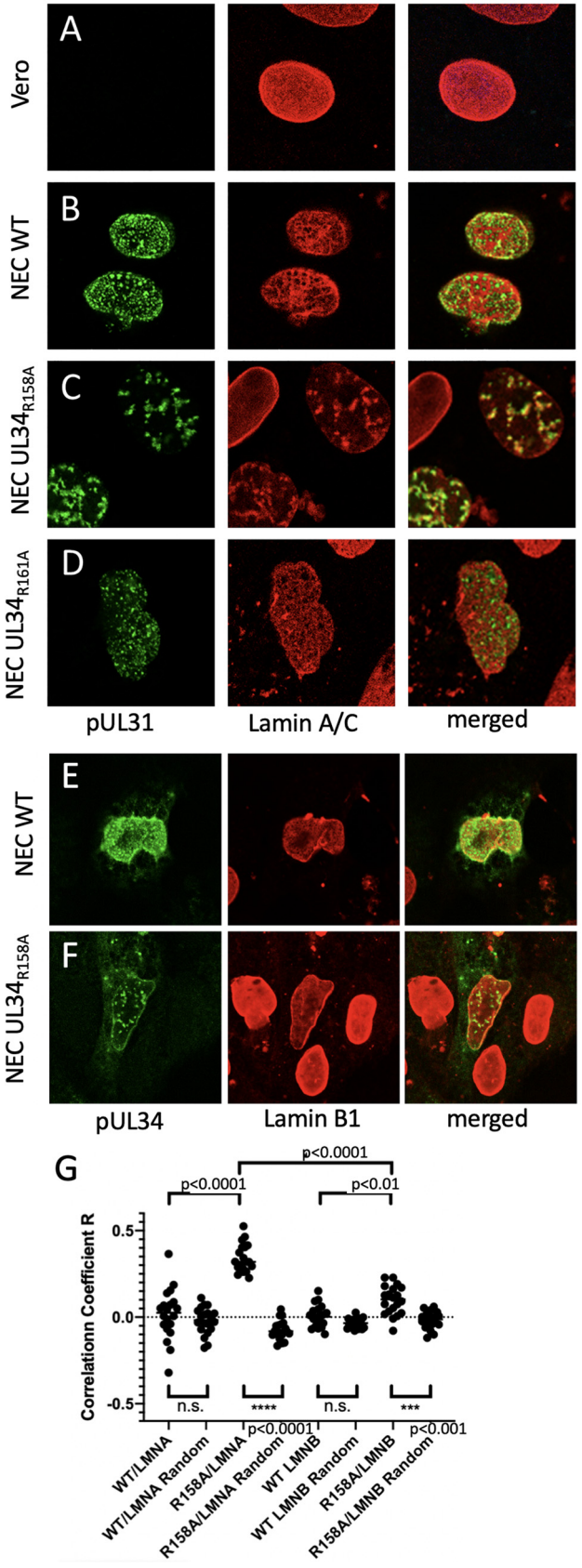

FIG 10 Lamina disruption by transiently expressed WT and mutant NEC. (A to D) Representative confocal images of cells that were either untransfected (A) or transfected with plasmids expressing

(Continued on next page)

protein kinase that can be recruited by a WT NEC. Protein kinase C isoforms, including the classical isoforms PKCα and -β and the novel isoform PKCδ, have previously been shown to be recruited to the nuclear envelope during HSV infection in a NEC-dependent manner and are thought to promote dispersal of the lamina (20). While recruitment and activation of PKCδ has been shown to depend on expression of both the NEC and ICP34.5 (13), it has not been determined whether other viral factors are required for interaction with classical PKC isoforms. We were unable to observe in cotransfected cells significant colocalization of PKC isoforms with WT or mutant NEC (data not shown). We were, however, able to demonstrate an interaction between the NEC and PKCα by coimmunoprecipitation (Fig. 11). 293T cells were cotransfected with plasmids that express PKCα-HA, pUL31-FLAG, and either WT or mutant pUL34. As expected, immunoprecipitation of pUL31 resulted in efficient coprecipitation of pUL34 WT and pUL34$_{R161A}$ and relatively inefficient coprecipitation of pUL34$_{R158A}$ (Fig. 11). PKCα-HA was also coprecipitated and, surprisingly, the amount coprecipitated did not depend on whether WT or pUL34$_{R158A}$ proteins were expressed, suggesting the possibility that expression of pUL31 might be sufficient for interaction with PKCα. Indeed, cotransfection of PKCα with pUL31 alone resulted in the same degree of PKCα coprecipitation as pUL31 in combination with pUL34 (Fig. 11B).

DISCUSSION

We have previously characterized the UL34$_{R158A,R161A}$ charge cluster double mutant (called CL13) as having a profound, but not dominant-negative effect on virus replication and nuclear egress, associated with accumulation of empty vesicle in nuclear membrane invaginations (24). This observation suggested the hypothesis that UL34 (CL13) might cause promiscuous, capsidless budding and that this loss of regulation might so diminish the efficiency of nuclear egress as to result in the growth defect associated with this mutation. Later elucidation of the crystal structure of the intact NEC suggested that one of the two mutations (UL34$_{R158A}$) might perturb formation of the NEC heterodimer and that this perturbation might be the basis of the CL13 phenotype. The phenotypes shown here that are associated with the individual UL34$_{R158A}$ and UL34$_{R161A}$ mutants demonstrate that both of these hypotheses are wrong in important and interesting ways.

Effect of pUL34 mutations on NEC formation. Consistent with our previously published results, we found here that, in transfected cells, the CL13 double mutant is significantly impaired in its ability to form a heterodimer with pUL31. Interestingly, neither of the single mutants reproduces this phenotype; both are capable of colocalizing with pUL31 at the nuclear envelope and of being coprecipitated with pUL31. This result for pUL34$_{R161A}$ was not surprising, since the crystal structure of the HSV-1 NEC heterodimer does not suggest that R161 participates in any interaction with pUL31 (Fig. 1). The failure of the R158A mutation to perturb interaction with pUL31 in colocalization assays performed in Vero cells was more surprising, since (i) the position of R158 would allow formation of a salt bridge with pUL31 perturbation of this interaction might be expected to destabilize the heterodimer, and (ii) this mutation clearly impairs heterodimer formation in coimmunoprecipitation assays in 293T cells. Because 293T cells do not spread extensively in monolayer culture, use of microscopy to evaluate recruitment of pUL34 from the cytoplasm to the nuclear rim is not possible, but the

FIG 10 Legend (Continued)
pUL31-FLAG and WT (B and E) or mutant (C, D, and F) pUL34. At 48 h after transfection, the cells were fixed and stained with antibodies against FLAG epitope (green) (A to D), HA epitope (green) (E and F), lamin A/C (red) (A to D), or lamin B1 (red) (E and F). (E) Colocalization of pUL31 and lamin A/C assessed by Pearson correlation coefficient. Each point represents one cell, and 20 cells were used for each analysis. The results are presented in pairs; the left sample gives the correlation coefficient *R* for green and red channels in the nucleus, and the right sample gives the mean of the *R* values for 25 comparisons of the green channel to a red channel with the signal randomized using the method of Costes. Statistical significance was determined by one-way ANOVA using the Tukey method for multiple comparisons implemented with GraphPad Prism.

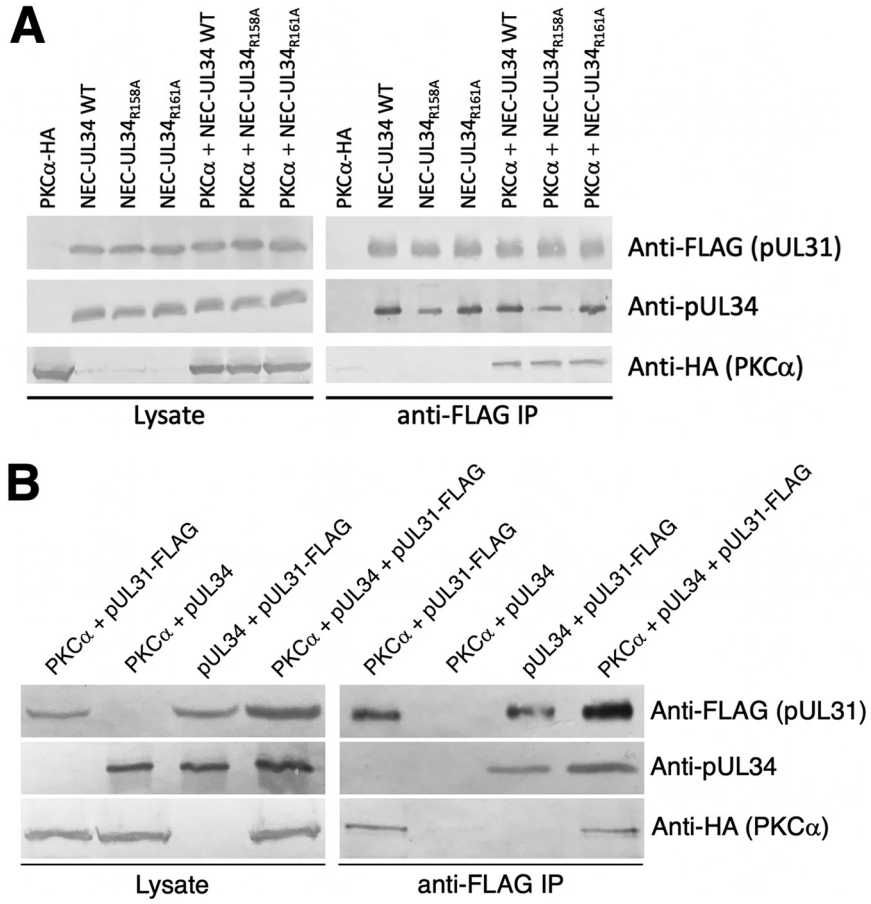

FIG 11 Interactions between wild-type and mutant NEC components and PKCα. (A) Coimmunoprecipitation of PKCα-HA and wild-type or mutant NEC. pUL31-FLAG was purified from 293T cells transfected with the indicated plasmid combinations. Immunoblots of cell lysates (left) and magnetic-bead purified samples (right) were incubated with antibodies against the pUL34 and HA or FLAG epitopes. (B) Coimmunoprecipitation of PKCα-HA and individual NEC components.

discrepancy between these results suggests that some cellular factor in Vero cells may stabilize the NEC. That both mutations together cause a significant disruption in Vero cells suggests the possibility that together they alter the conformation of the pUL34/pUL31interface in a way that neither mutation can do alone. Modeling the conformation of the CL13 double mutant using SWISS-MODEL (29) with the wild-type NEC as the template, however, results in a conformation prediction that is not different from that of the wild-type (not shown), leaving the structural basis for the heterodimer formation phenotype unclear.

Interestingly, while pUL34(CL13) interaction with pUL31 is severely impaired in cotransfected cells, its recruitment to the nuclear envelope occurs more efficiently in infected cells (compare Fig. 2 and 3), and this occurs despite relatively inefficient recruitment of pUL31 from the nucleoplasm to the nuclear membrane (Fig. 3). This result suggests that recruitment of pUL34 to the nuclear envelope is promoted by viral factors in addition to pUL31. A similar effect has also been observed for specific pUL34 mutations in PRV (28). Whether the nuclear membrane recruitment of pUL34(CL13) occurs independently of pUL31 or results from promotion of interaction between the mutant pUL34 and pUL31 is not clear. The occurrence of promiscuous membrane budding in infected cells that express pUL34(CL13), however, suggests that NEC heterodimers form to a degree sufficient to induce membrane budding in the INM.

Promiscuous budding and the efficiency of nuclear egress. Our initial hypothesis was that pUL34(CL13) was defective in regulation of budding and that this failure of

regulation resulted in inefficient nuclear egress and consequent diminished virus production. While pUL34(CL13) may indeed be defective in budding regulation, the $UL34_{R158A}$ and $UL34_{R161A}$ single mutations maintain the promiscuous budding phenotype of UL34 (CL13) without significantly impairing virus production or cell-cell spread, indicating that this negative regulation does not affect HSV-1 replication.

Interestingly, accumulations of capsid-less intranuclear vesicles similar to those observed here have also been observed as a phenotype of UL31 point mutants that alter amino acids at the apex of the NEC that would be expected to mediate interaction with the capsid (30). This similarity is consistent with two possibilities. (i) What we have interpreted as unregulated budding is, in fact, budding that is triggered by capsid interaction with the NEC, but this interaction is too weak to mediate stable association of capsids with the INM, resulting in empty vesicles. The position of the CL13 amino acid substitutions (Fig. 1) does not intuitively suggest an effect on capsid binding since it is well below the apex of the NEC, but these mutations may have subtle effects on the overall conformation of the NEC that might affect the stability of capsid binding. (ii) What others have interpreted as a failure of capsid docking is, in fact, a defect in budding regulation by the NEC. Structural characterization of the CL13 mutant could presumably help distinguish these possibilities.

pUL34 has been shown to affect both virus single-step growth, presumably due to its function in nuclear egress, and cell-to-cell spread by an unknown mechanism. The CL13 double mutation affects both of these processes (Fig. 5 and 6). Interestingly, the CL13 double mutation causes a severe cell-cell spread defect, whereas the single R158A mutation has no effect on spread (Fig. 6). Surprisingly, there is only a 1-log decrease in virus production of UL34(CL13) compared to $UL34_{R158A}$, confirming the conclusion of other studies showing that that the single-step growth of HSV does not reliably predict its ability to spread from cell to cell (27, 31, 32).

$UL34_{R158A}$ mutation and the lamina disruption activity of the NEC. Coexpression of pUL31 and pUL34 in the absence of other viral proteins creates gaps in the lamin A/C network that correspond to the position of NEC puncta (Fig. 8). This is not simply an artifact of protein overexpression, since the single R158A amino acid substitution in pUL34 prevents removal of lamin A/C from sites of NEC accumulation and, in fact, results in concentration of lamin A/C at these sites. These observations are consistent with a model in which the HSV-1 NEC, in the absence of other viral factors, either has an intrinsic lamin dispersal activity or can recruit cellular factors such as protein kinases for lamina dispersal. In the absence of that dispersal activity, lamins can stably associate with the NEC. The stable association of lamins with the NEC is consistent with a previous demonstration of interaction between lamin A/C and pUL34 (19). It has also been previously shown that PKC isoforms are recruited to the nuclear rim in an NEC-dependent manner in infected cells (20). This idea is consistent with previous findings showing interaction of pUL34 and lamin A/C (19) and recruitment of PKC isoforms by the NEC that might disassemble lamin filaments (7, 13, 20). The mechanism by which the R158A mutation in pUL34 prevents lamina dispersal in transfected cells is not clear. The NEC cannot efficiently recruit PKCδ in the absence of ICP34.5, suggesting that this kinase is unlikely to be the mediator of lamina dispersal in transfected cells (13). Our results demonstrate that interaction with PKCα relies only on the presence of pUL31. It may be that simple recruitment of PKCα is insufficient and that WT pUL34 is required for its activation at the nuclear envelope.

The roughly 10-fold growth defect associated with the $UL34_{R158A}$ mutant is consistent with a previously characterized $UL34_{Q163A}$ mutant with a defect in lamina disruption (17). The similarity in the magnitude of growth and spread defect between $UL34_{R158A}$ and $UL34_{Q163A}$/$UL31_{R229L}$ suggests that an intact viral lamin disruption mechanism is helpful but perhaps not essential for viral assembly and spread.

MATERIALS AND METHODS

Cells and viruses. Vero cells and cell lines derived from Vero cells were maintained in Dulbecco modified Eagle medium (high glucose; DMEM) supplemented with 5% bovine calf serum. 293T cells

were maintained in DMEM supplemented with 10% fetal bovine serum. The properties of HSV-1(F), bacterial artificial chromosome (BAC)-derived HSV-1(F), vRR1072(TK$^+$) (referred to here as UL34-null virus), BAC-derived UL34-null virus, UL31(R229L)-FLAG/UL34-null, and HSV-1(F)/RFP-UL35 have been described previously (25, 33–35). The RFP-UL35/UL34-null virus was generated using BAC recombineering to delete UL34 from the RFP-UL35 virus (33; a gift from C. Fraefel) using the PCR primers and procedures used for generation of the previously described BAC-derived UL34-null virus (25).

Plasmids and cell lines. pcDNA plasmids carrying wt UL34 (pRR1238) and UL31-FLAG (pRR1334) was described previously (25). pcDNA3 plasmids carrying N-terminally HA-tagged UL34 (pRR1385) or HA-tagged UL34(CL13) (pRR1386) were constructed by the amplification of the UL34 coding sequence from pRR1300 (containing UL34 coding sequence) or pRR1369 (containing UL34(CL13 coding sequence) using the primers 5′-GATCAAGCTTCCATGTACCCATACGATGTTCCAGATTACGCTGCGGGACTGGGCAAGCC C-3′ and 5′-CTAGTCTAGATTATAGGCGCGCGCCAGC-3′, digestion of the resulting PCR product with HindIII and AflII, and ligation into HindIII-AflII-cut pRR1238.

pcDNA3 plasmids carrying N-terminally, HA-tagged UL34$_{R158A}$ (pRR1387) or UL34$_{R161A}$ (pRR1388) were constructed by introduction of the R158A or R161A mutation into the coding sequence of UL34 by PCR stitching. The primers 5′-GATCAAGCTTCCATGTACCCATACGATGTTCCAGATTACGCTGCGGGACTGGG CAAGCCC-3′, 5′-CACAAAGCAGCTGATCCACATGCTG-3′, 5′-CATGTGGATCAGCTGCTTTGTGGCCATGCCCCG CGTGCAGC-3′, and 5′-CTAGTCTAGATTATAGGCGCGCGCCAGC-3′ were used to create the UL34$_{R158A}$ mutant coding sequence, and the primers 5′-GATCAAGCTTCCATGTACCCATACGATGTTCCAGATTACGCTG CGGGACTGGGCAAGCCC-3′, 5′-TGCAGGCATGCGCACAAAGC-3′, 5′-GCTTTGTGCGCATGCCTGCAGTGCAGC TCGCGTTTCGGTTC-3′, and 5′-CTAGTCTAGATTATAGGCGCGCGCCAGC-3′ were used to construct the UL34$_{R161A}$ mutant coding sequence. The resulting PCR products were digested with HindIII and AflII and ligated into HindIII-AflII-cut pRR1238.

Infection inducible UL34$_{R158A}$-expressing or UL34$_{R161A}$-expressing plasmids were constructed. The UL34$_{R158A}$ and UL34$_{R161A}$ coding sequences were amplified from pRR1387 and pRR1388, respectively, and inserted into pTuner-IRES2 (Clontech) using Gibson assembly. The resulting plasmids express bicistronic pUL34$_{R158A}$-IRES2-EGFP or pUL34$_{R161A}$-IRES2-EGFP mRNA from the UL34 promoter/regulatory sequences.

A plasmid that expresses PKCα from the vector pHACE was kindly provided by I. Bernard Weinstein (38). Stable Vero cell lines that express wild-type pUL34 and pUL34 (CL13) have been previously described (24, 25). The UL34$_{R158A}$ and the UL34$_{R161A}$ clonal cell lines (referred to here as R158A and R161A cells, respectively) were constructed as described previously (24, 25), with some modifications. Briefly, transfection of infection inducible UL34$_{R158A}$-expressing or UL34$_{R161A}$-expressing plasmids into Vero cells was followed by selection with G418 and isolation of clones by limited dilution. Candidate R158A cells or R161A cells were identified by their enhanced green fluorescent protein expression 15 h after infection with HSV-1(F). Expression of pUL34$_{R158A}$ or pUL34$_{R161A}$ was confirmed by immunofluorescence and immunoblotting for pUL34 15 h after infection with BAC-derived UL34-null virus.

Complementation assay. Next, 24-well cultures of Vero cells were transfected with 125 ng of pCMVβ, expressing the β-galactosidase gene, and 125 ng of wild-type or mutant UL34 plasmid with Lipofectamine reagent according to the manufacturer's protocol (Gibco-BRL), followed by incubation overnight at 37°C. The cells were then infected with UL34-null virus at an MOI of 10, followed by incubation at 37°C for 90 min. Monolayers were washed three times with DMEM and then washed three times with sodium citrate buffer pH 3 (50 mM sodium citrate and 4 mM potassium chloride adjusted to pH 3 with hydrochloric acid) to eliminate residual virus. Cells were washed with V medium (Dulbecco modified Eagle medium, penicillin-streptomycin, 1% heat-inactivated calf serum) until the pH returned to a normal level.

One milliliter of V medium was added to each well; after 18 h of incubation at 37°C, cell lysates were prepared by freezing and thawing, followed by sonication for 20 s at power level 2 with a Fisheronic dismembrator. The amount of infectivity in each lysate was determined by titration on Vero cells. Part of each cell lysate was assayed for β-galactosidase expression as described previously (26).

Coimmunoprecipitation. 293T cells in 100 mm dishes were transfected with plasmids pRR1385 (HA-UL34), pRR1386 (HA-UL34(CL13), pRR1387 (HA-UL34$_{R158A}$), pRR1388 (HA-UL34$_{R161A}$), pRR1334 (UL31-FLAG), pcDNA3, or pHACE-PKCα-HA by use of polyethyleneimine (PEI). A total of 9 μg of plasmid was diluted into 500 μl of DMEM with no additives (DMEM/NA) and then mixed with 500 ml of DMEM/NA containing 81 μg of PEI. After incubation at room temperature for 15 min to allow complexes to form, the mixture was added to cultures of 50% confluent cells that had been seeded 24 h previously. After 48 h, transfected cells were washed once in phosphate-buffered saline (PBS), scraped into 5 ml of fresh PBS, and pelleted at 800 $\times$ *g* for 10 min. Cells were lysed by resuspension of the cell pellet in RIPA buffer (50 mM Tris [pH 7.5], 150 mM NaCl, 1 mM EDTA, 1% Triton X-100, 5 mM sodium vanadate, 5 mM NaF), followed by sonication. After the removal of 60 μl of input control sample, the remainder was immunoprecipitated with 8 μl of anti-FLAG M2 magnetic resin (Sigma) according to the manufacturer's instructions by using an overnight binding step and elution with 3$\times$FLAG peptide. Input and immunoprecipitation samples were separated in 10% SDS-PAGE gels and blotted onto nitrocellulose membranes.

Immunoblotting. Nitrocellulose sheets containing proteins of interest were blocked in 5% nonfat milk plus 0.2% Tween 20 for at least 45 min. Membranes were probed with the following primary antibodies: chicken anti-pUL34 (36), mouse monoclonal anti-ICP27 (Virusys), mouse monoclonal anti-FLAG M2 (Sigma), and mouse monoclonal anti-HA (BioLegend). The membranes were then incubated with the respective alkaline phosphatase-conjugated secondary antibody.

Indirect immunofluorescence. Cells were fixed with 4% formaldehyde for 15 min and then washed in PBS. Cells were permeabilized and blocked by incubation in IF buffer (1$\times$ PBS, 0.5% Triton X-100, 0.5% sodium deoxycholate, 1% egg albumin, 0.01% NaN_3). Primary antibodies were diluted in IF buffer as

follows: chicken anti-UL34, 1:500; mouse anti-FLAG M2 (Sigma), 1:500; mouse monoclonal anti-LMNA (Santa Cruz Biotechnology), 1:500; goat anti-lamin B1 (Santa Cruz Biotechnology), 1:200; and mouse anti-MYC (kind gift from Mike Apicella), 1:500. Cellular DNA was stained with Hoechst 33342 (Invitrogen). Coverslips were mounted onto glass slides, and confocal microscopy was performed using a Zeiss 510 confocal microscope or Leica SPE. All images shown are representative of experiments performed a minimum of three times.

Colocalization assays. For colocalization of pUL31 and pUL34 mutants in transfected cells, 24 wells of Vero cells containing coverslips were transfected with pcDNA3 plasmids carrying UL31-FLAG (pRR1334), HA-UL34 (pRR1385), HA-UL34(CL13) (pRR1386), $UL34_{R158A}$ (pRR1387), HA-$UL34_{R161A}$ (pRR1388), or MYC-US3 using Lipofectamine reagent according to the manufacturer's instructions. Samples were harvested for indirect immunofluorescence 2 days posttransfection. Confocal images of 20 cells were taken with the Leica SPE, and the Pearson's correlation coefficient was determined using ImageJ.

For colocalization of NEC and lamins in transfected cells, 24-well cultures of Vero cells on coverslips were transfected with pRR1334 and pRR1385, pRR1386, pRR1387, or pRR1388 and then fixed at 48 h after transfection. Confocal images of 20 cells were taken with the Leica SPE and colocalization was determined by defining the cell nucleus as a region of interest and using the ImageJ colocalization test using the Costes method for image randomization (37) and 25 iterations for each cell.

For colocalization of pUL31 and pUL34 under infectious conditions, Vero cells, UL34-expressing, CL13-expressing, R158A-expressing, and R161A-expressing cells were infected with BAC-derived UL34-null virus. Samples were prepared for indirect immunofluorescence at 15 hpi.

Plaque size assays. Twelve-well tissue culture plates were seeded with 5×10^5 Vero cells the day before infection. Cells were infected at a low MOI for 1.5 h, and then the virus inoculum was replaced with a 1:250 dilution of pooled human immunoglobulin (GammaSTAN) in V medium. Cells were fixed and stained after 2 days of infection. A mouse monoclonal anti-HSV 45-kDa protein (scaffolding protein) antibody (Serotec) and Alexa Fluor 568–goat anti-mouse IgG (Invitrogen) were used as primary and secondary antibodies, respectively.

Single-step growth measurements. Measurement of replication of BAC-derived HSV-1(F) and BAC-derived UL34-null viruses on Vero, UL34-expressing, CL13-expressing, R158A-expressing, or R161A-expressing cells was performed as previously described (36).

Transmission electron microscopy of infected cells. Confluent monolayers of UL34WT-expressing, CL13-expressing, R158A-expressing, and R161A-expressing cells were infected with UL34-null virus (1072 TK^+) at an MOI of 5 in V medium for 20 h and then fixed by incubation in 2.5% glutaraldehyde in 0.1 M cacodylate buffer (pH 7.4) for 2 h. Cells were postfixed in 1% osmium tetroxide, washed in cacodylate buffer, embedded in Spurr's resin, and cut into 95-nm sections. Sections were mounted on grids, stained with uranyl acetate and lead citrate, and then examined with a JEOL 1250 transmission electron microscope. Ten cells were used for the quantitation of viral capsids within cellular compartments. DNA-containing and non-DNA-containing capsids were counted in the nucleus, the perinuclear space (between the INM and the ONM), and the extranuclear compartment (within the cytoplasm or the extracellular space).

RFP maximum assay. A total of 24 wells containing coverslips of Vero, UL34-expressing, CL13-expressing, R158A-expressing, or R161A-expressing cells were infected with either UL35-RFP/HSV-1(F) or UL35-RFP/UL34-null virus in V medium at an MOI of 5. At 12 hpi, CellTracker Green BODIPY (ThermoFisher) was added to a concentration of 25 micromolars, and incubation was continued for 30 min. Cells were then fixed and prepared for indirect immunofluorescence. In confocal images, CellTracker Green staining and Hoechst 33342 staining were used to define the nuclear and cytoplasmic boundaries of the cell, respectively. ImageJ was used to count the number of RFP maxima, or points where the RFP intensity is the highest, in the cytoplasm.

ACKNOWLEDGMENTS

This study was supported by NIAID R21AI133155. A.V. was supported by NIAID T32AI007533. T.C. was supported by NSF DBI-1559927.

We are grateful to Cornel Fraefel for the gift of the mRFP-UL35 fusion virus. We also thank Alison Haugo and Masoudeh Masoud Bahnamiri for critical reading of the manuscript.

REFERENCES

1. Roller RJ, Baines JD. 2017. Herpesvirus nuclear egress. Adv Anat Embryol Cell Biol 223:143–169. https://doi.org/10.1007/978-3-319-53168-7_7.
2. Bigalke JM, Heldwein EE. 2015. Structural basis of membrane budding by the nuclear egress complex of herpesviruses. EMBO J 34:2921–2936. https://doi.org/10.15252/embj.201592359.
3. Bigalke JM, Heuser T, Nicastro D, Heldwein EE. 2014. Membrane deformation and scission by the HSV-1 nuclear egress complex. Nat Commun 5. https://doi.org/10.1038/ncomms5131.
4. Hagen C, Dent KC, Zeev-Ben-Mordehai T, Grange M, Bosse JB, Whittle C, Klupp BG, Siebert CA, Vasishtan D, Bäuerlein FJ, Cheleski J, Werner S, Guttmann P, Rehbein S, Henzler K, Demmerle J, Adler B, Koszinowski U, Schermelleh L, Schneider G, Enquist LW, Plitzko JM, Mettenleiter TC, Grünewald K. 2015. Structural basis of vesicle formation at the inner nuclear membrane. Cell 163:1692–1701. https://doi.org/10.1016/j.cell.2015.11.029.
5. Bjerke SL, Roller R. 2006. Roles for herpes simplex type 1 UL34 and US3 proteins in disrupting the nuclear lamina during herpes simplex virus type 1 egress. Virology 347:261–276. https://doi.org/10.1016/j.virol.2005.11.053.
6. Leach N, Bjerke SL, Christensen DK, Bouchard JM, Mou F, Park R, Baines J, Haraguchi T, Roller RJ. 2007. Emerin is hyperphosphorylated and redistributed in herpes simplex virus type 1-infected cells in a manner dependent on both UL34 and US3. J Virol 81:10792–10803. https://doi.org/10.1128/JVI.00196-07.
7. Leach NR, Roller RJ. 2010. Significance of host cell kinases in herpes simplex virus type 1 egress and lamin-associated protein disassembly from

the nuclear lamina. Virology 406:127–137. https://doi.org/10.1016/j.virol.2010.07.002.
8. Liu Z, Kato A, Oyama M, Kozuka-Hata H, Arii J, Kawaguchi Y. 2015. Role of host cell p32 in herpes simplex virus 1 de-envelopment during viral nuclear egress. J Virol 89:8982–8998. https://doi.org/10.1128/JVI.01220-15.
9. Liu Z, Kato A, Shindo K, Noda T, Sagara H, Kawaoka Y, Arii J, Kawaguchi Y. 2014. Herpes simplex virus 1 UL47 interacts with viral nuclear egress factors UL31, UL34, and Us3 and regulates viral nuclear egress. J Virol 88:4657–4667. https://doi.org/10.1128/JVI.00137-14.
10. Maruzuru Y, Shindo K, Liu Z, Oyama M, Kozuka-Hata H, Arii J, Kato A, Kawaguchi Y. 2014. Role of herpes simplex virus 1 immediate early protein ICP22 in viral nuclear egress. J Virol 88:7445–7454. https://doi.org/10.1128/JVI.01057-14.
11. Reynolds AE, Wills EG, Roller RJ, Ryckman BJ, Baines JD. 2002. Ultrastructural localization of the herpes simplex virus type 1 UL31, UL34, and US3 proteins suggests specific roles in primary envelopment and egress of nucleocapsids. J Virol 76:8939–8952. https://doi.org/10.1128/jvi.76.17.8939-8952.2002.
12. Ryckman BJ, Roller RJ. 2004. Herpes simplex virus type 1 primary envelopment: UL34 protein modification and the US3-UL34 catalytic relationship. J Virol 78:399–412. https://doi.org/10.1128/jvi.78.1.399-412.2004.
13. Wu S, Pan S, Zhang L, Baines J, Roller R, Ames J, Yang M, Wang J, Chen D, Liu Y, Zhang C, Cao Y, He B. 2016. Herpes simplex virus 1 induces phosphorylation and reorganization of lamin A/C through the γ134.5 protein that facilitates nuclear egress. J Virol 90:10414–10422. https://doi.org/10.1128/JVI.01392-16.
14. Barton LJ, Wilmington SR, Martin MJ, Skopec HM, Lovander KE, Pinto BS, Geyer PK. 2014. Unique and shared functions of nuclear lamina LEM domain proteins in *Drosophila*. Genetics 197:653–665. https://doi.org/10.1534/genetics.114.162941.
15. de Leeuw R, Gruenbaum Y, Medalia O. 2018. Nuclear lamins: thin filaments with major functions. Trends Cell Biol 28:34–45. https://doi.org/10.1016/j.tcb.2017.08.004.
16. Muranyi W, Haas J, Wagner M, Krohne G, Koszinowski UH. 2002. Cytomegalovirus recruitment of cellular kinases to dissolve the nuclear lamina. Science 297:854–857. https://doi.org/10.1126/science.1071506.
17. Vu A, Poyzer C, Roller R. 2016. Extragenic suppression of a mutation in herpes simplex virus 1 UL34 that affects lamina disruption and nuclear egress. J Virol 90:10738–10751. https://doi.org/10.1128/JVI.01544-16.
18. Morris JB, Hofemeister H, O'Hare P. 2007. Herpes simplex virus infection induces phosphorylation and delocalization of emerin, a key inner nuclear membrane protein. J Virol 81:4429–4437. https://doi.org/10.1128/JVI.02354-06.
19. Mou F, Wills EG, Park R, Baines JD. 2008. Effects of lamin A/C, lamin B1, and viral US3 kinase activity on viral infectivity, virion egress, and the targeting of herpes simplex virus U(L)34-encoded protein to the inner nuclear membrane. J Virol 82:8094–8104. https://doi.org/10.1128/JVI.00874-08.
20. Park R, Baines J. 2006. Herpes simplex virus type 1 infection induces activation and recruitment of protein kinase C to the nuclear membrane and increased phosphorylation of lamin B. J Virol 80:494–504. https://doi.org/10.1128/JVI.80.1.494-504.2006.
21. Scott ES, O'Hare P. 2001. Fate of the inner nuclear membrane protein lamin B receptor and nuclear lamins in herpes simplex virus type 1 infection. J Virol 75:8818–1830. https://doi.org/10.1128/JVI.75.18.8818-8830.2001.
22. Simpson-Holley M, Colgrove RC, Nalepa G, Harper JW, Knipe DM. 2005. Identification and functional evaluation of cellular and viral factors involved in the alteration of nuclear architecture during herpes simplex virus 1 infection. J Virol 79:12840–12851. https://doi.org/10.1128/JVI.79.20.12840-12851.2005.
23. Klupp BG, Granzow H, Fuchs W, Keil GM, Finke S, Mettenleiter TC. 2007. Vesicle formation from the nuclear membrane is induced by coexpression of two conserved herpesvirus proteins. Proc Natl Acad Sci U S A 104:7241–7246. https://doi.org/10.1073/pnas.0701757104.
24. Roller RJ, Haugo AC, Kopping NJ. 2011. Intragenic and extragenic suppression of a mutation in herpes simplex virus-1 UL34 that affects both nuclear envelope targeting and membrane budding. J Virol 85:11615–11625. https://doi.org/10.1128/JVI.05730-11.
25. Roller RJ, Bjerke SL, Haugo AC, Hanson S. 2010. Analysis of a charge cluster mutation of herpes simplex virus type 1 UL34 and its extragenic suppressor suggests a novel interaction between pUL34 and pUL31 that Is necessary for membrane curvature around capsids. J Virol 84:3921–3934. https://doi.org/10.1128/JVI.01638-09.
26. Bjerke SL, Cowan JM, Kerr JK, Reynolds AE, Baines JD, Roller RJ. 2003. Effects of charged cluster mutations on the function of herpes simplex virus type 1 U_L34 protein. J Virol 77:7601–7610. https://doi.org/10.1128/jvi.77.13.7601-7610.2003.
27. Haugo AC, Szpara ML, Parsons L, Enquist LW, Roller RJ. 2011. Herpes simplex virus 1 pUL34 plays a critical role in cell-to-cell spread of virus in addition to its role in virus replication. J Virol 85:7203–7215. https://doi.org/10.1128/JVI.00262-11.
28. Passvogel L, Janke U, Klupp BG, Granzow H, Mettenleiter TC. 2014. Identification of conserved amino acids in pUL34 which are critical for function of the pseudorabies virus nuclear egress complex. J Virol 88:6224–6231. https://doi.org/10.1128/JVI.00595-14.
29. Waterhouse A, Bertoni M, Bienert S, Studer G, Tauriello G, Gumienny R, Heer FT, de Beer TAP, Rempfer C, Bordoli L, Lepore R, Schwede T. 2018. SWISS-MODEL: homology modeling of protein structures and complexes. Nucleic Acids Res 46:W296–W303. https://doi.org/10.1093/nar/gky427.
30. Takeshima K, Arii J, Maruzuru Y, Koyanagi N, Kato A, Kawaguchi Y. 2019. Identification of the capsid binding site in the herpes simplex virus 1 nuclear egress complex and its role in viral primary envelopment and replication. J Virol 93:e01290-19. https://doi.org/10.1128/JVI.01290-19.
31. Feutz E, McLeland-Wieser H, Ma J, Roller RJ. 2019. Functional interactions between herpes simplex virus pUL51, pUL7 and gE reveal cell-specific mechanisms for epithelial cell-to-cell spread. Virology 537:84–96. https://doi.org/10.1016/j.virol.2019.08.014.
32. Roller RJ, Haugo AC, Yang K, Baines JD. 2014. The herpes simplex virus 1 UL51 gene product has cell type-specific functions in cell-to-cell spread. J Virol 88:4058–4068. https://doi.org/10.1128/JVI.03707-13.
33. de Oliveira AP, Glauser DL, Laimbacher AS, Strasser R, Schraner EM, Wild P, Ziegler U, Breakefield XO, Ackermann M, Fraefel C. 2008. Live visualization of herpes simplex virus type 1 compartment dynamics. J Virol 82:4974–4990. https://doi.org/10.1128/JVI.02431-07.
34. Ejercito PM, Kieff ED, Roizman B. 1968. Characteristics of herpes simplex virus strains differing in their effect on social behavior of infected cells. J Gen Virol 2:357–364. https://doi.org/10.1099/0022-1317-2-3-357.
35. Tanaka M, Kagawa H, Yamanashi Y, Sata T, Kawaguchi Y. 2003. Construction of an excisable bacterial artificial chromosome containing a full-length infectious clone of herpes simplex virus type 1: viruses reconstituted from the clone exhibit wild-type properties *in vitro* and *in vivo*. J Virol 77:1382–1391. https://doi.org/10.1128/jvi.77.2.1382-1391.2003.
36. Roller RJ, Zhou Y, Schnetzer R, Ferguson J, DeSalvo D. 2000. Herpes simplex virus type 1 U_L34 gene product is required for viral envelopment. J Virol 74:117–129. https://doi.org/10.1128/jvi.74.1.117-129.2000.
37. Costes SV, Daelemans D, Cho EH, Dobbin Z, Pavlakis G, Lockett S. 2004. Automatic and quantitative measurement of protein-protein colocalization in live cells. Biophys J 86:3993–4003. https://doi.org/10.1529/biophysj.103.038422.
38. Soh JW, Weinstein IB. 2003. Roles of specific isoforms of protein kinase C in the transcriptional control of cyclin D1 and related genes. J Biol Chem 278:34709–34716. https://doi.org/10.1074/jbc.M302016200.